Journal of Translational Medicine

RESEARCH

Open Access

A live tumor fragment platform to assess immunotherapy response in core needle biopsies while addressing challenges of tumor heterogeneity

T. S. Ramasubramanian[1], Pichet Adstamongkonkul[1], Christina M. Scribano[1], Christin Johnson[1], Sean Caenepeel[1], Laura C.F. Hrycyniak[1], Lindsey C. Vedder[1], Nicholas Dana[1], Christian Baltes[1], Victoria Browning[1], Yuan-I Chen[1], Thomas Dietz[1], Evan Flietner[1], Nicholas Kaplewski[1], Anna Kellner[1], Michael Korrer[1], Chao Liu[1], Nathan Marhefke[1], Payton McDonnell[1], Amreen Nasreen[1], Victoria Pope[1], Abhijeet Prasad[1^], Jordyn Richardson[1], Sidney Schneider[1], Mikaela M. Schultz[1], Chetan Sood[1], Aishwarya Sunil[1], Erika von Euw[1], Eric Wait[1], Ellen E. Wargowski[1], Pooja Advani[2], Barbara Broome[3], Antje Bruckbauer[4], Andrew Godwin[5], Nima Kokabi[6], Yanyan Lou[2], Robert C. G. Martin 2nd[7], Mercedes Robaina[8], Giuseppe Toia[9], Joshua Routh[10], Andreas Friedl[9], Kevin Eliceiri[9], Michael Szulczewski[1], Scott Johnson[1], Jon Oliner[1], Jérôme Galon[11], Christian Capitini[9], Debabrata Mukhopadhyay[2], Janis Taube[12], David Braun[13] and Hinco J. Gierman[1*]

Abstract

Background Immune checkpoint inhibitors (ICIs) have revolutionized cancer treatment, providing durable and even curative responses. However, most patients do not respond and current biomarkers (eg, programmed death 1 ligand 1 [PD-L1]), mismatch repair deficiency [dMMR]/high microsatellite instability [MSI] and tumor mutational burden) lack predictive accuracy. Ex vivo profiling of patient-derived tumor fragments shows promise as a predictive biomarker but relies on substantial surgical tissue to mitigate intra-specimen heterogeneity. Innovations are needed that address these challenges, particularly where limited tissue is available such as in core needle biopsies (CNBs).

Methods Live tumor fragments (LTFs) were generated from 59 human tumor resections and 31 CNBs from patients enrolled in observational clinical trials (ClinicalTrials.gov identifiers: NCT05478538, NCT05520099, NCT06349642) to assess cytokine induction following ICI treatment. LTFs were encapsulated in hydrogel and cultured ex vivo for up to 72 hours. A sequential treatment strategy that applies control and treatment within the same well was used with

[†]In memory of Abhijeet Prasad.

*Correspondence:
Hinco J. Gierman
cso@elephas.com

Full list of author information is available at the end of the article

response to ICI or αCD3/αCD28 assessed using a multiplex secretome assay. Viability was assessed using established metabolic assays and dynamic optical coherence microscopy.

Results LTFs maintained viability and retained T cells responsive to stimulation throughout ex vivo culture. Multiplex immunofluorescence and immunohistochemistry showed key components of the tumor microenvironment, including relative proportions of $CD4^+$ and $CD8^+$ immune cell populations, were preserved. Specimens positive for PD-L1 or dMMR/MSI-high were enriched for cytokine upregulation, including T-cell response cytokines IFNγ and CXCL10, after αPD-1 treatment. To demonstrate clinical applicability of the sequential treatment strategy, CNBs from patients with lung, gastrointestinal or kidney cancer were profiled and differential cytokine induction in response to ICI treatment was observed.

Conclusions The novel ex vivo platform presented is capable of detecting T-cell response to ICI treatment by using a sequential treatment strategy. This approach addresses challenges associated with cross-well heterogeneity in tissue composition and requires half as much tissue as a cross-well comparison, mitigating tissue limitations typically associated with non-surgical biopsies. Importantly, the platform is compatible with established functional assays as well as non-destructive spatial imaging, enabling researchers to characterize response to ICI longitudinally. Ongoing trials will enable clinicians to assess platform performance in predicting response to immunotherapy.

Background

Immune checkpoint inhibitors (ICIs) have revolutionized cancer therapy, yielding unprecedented clinical benefits for a subset of patients, including curative responses for patients with several types of advanced/metastatic tumors [1]. Currently, 3 clinically validated biomarkers are US Food and Drug Administration (FDA) approved to predict patient response to ICI treatment; programmed death 1 ligand 1 (PD-L1) expression [2–6], microsatellite instability (MSI)/mismatch repair deficiency (dMMR) [5, 7], and tumor mutational burden [8]. Nearly 50% of patients with cancer in the US are not ICI-eligible based on these biomarkers [9]. Moreover, of those receiving treatment, only 20% to 30% obtain an objective response [9, 10], underscoring the limited predictive ability of available biomarkers. While anti-programmed cell death 1 (αPD-1) antibody treatment is generally well tolerated, 10% of patients experience severe immune-related adverse events, including fatalities in 0.6% of patients [11, 12]. Thus, accurate identification of patients likely to benefit from ICI therapy is critical to optimize clinical outcomes and minimize harm, highlighting the need for more robust, reliable, and functionally informative approaches to identify ICI responders.

Ex vivo systems that use live tissues while preserving the native architecture and tumor microenvironment (TME) offer powerful platforms for preclinical studies [13–15] and have shown promise in predicting therapeutic response [16–18]. Jenkins et al. demonstrated cytokine response to PD-1 and cytotoxic T-lymphocyte associated protein 4 (CTLA-4) inhibition in patient-derived organotypic tumor spheroids that maintained TME components, such as tumor stroma and immune cells [13]. Voabil et al. demonstrated that a classifier of cytokine response to ICI in tumor resections can predict the response to αPD-1 treatment in patients with cancer with high accuracy in a validation data set [16]. However, a key challenge in ex vivo ICI studies is the need for large amounts of tissue to overcome the inherent intra-tumor heterogeneity in the tissue sampled, which leads to unequal tissue composition during tissue allocation for cross-well comparisons. Density and viability of immune and tumor cells can vary drastically across a tumor, resulting in significant variations in cellular composition and microenvironmental conditions between samples of the same tumor specimen [19–21]. This can be problematic with the limited tissue available from a single core needle biopsy (CNB), which is the standard of care clinical diagnostic procedure for patients with advanced-stage metastatic disease who are not surgical candidates and are commonly treated with immunotherapy. Therefore, mitigating intra-specimen variability in tissue composition is essential for reliable ex vivo ICI response assessment.

The optimal platform for assessing ICI response would use live tissue with contiguous TME to enable spatial analysis—such as longitudinal, label-free advanced imaging—and functional response to treatment while eliminating the confounding factor of intra-specimen variability from the limited tissue amounts typical of standard practice diagnostic methods. Here, a novel ex vivo platform was developed for reliable ICI response analysis in CNBs using live tumor fragments (LTFs) designed to balance the preservation of a functional TME and mitigation of intra-specimen variability.

Methods

Methods are summarized below; see detailed methodology in the online Supplementary Material 1.

Specimens

Mouse models

Experiments using murine models were performed in accordance with the Institutional Animal Care and Use Committee approved protocol (23–003) in an Association for Assessment and Accreditation of Laboratory Animal Care International accredited laboratory per the eighth edition of the Guide for Care and Use of Laboratory Animals [22]. Tumors were removed through a terminal surgical procedure at a volume of 300–500 mm^3.

Syngeneic CT26

Mouse cell line CT26 (5 x 10^5 cells, ATCC, CRL-2638) were injected subcutaneously into one or both flanks of female BALB/c mice (The Jackson Laboratory) between 7 and 8 weeks of age. Cells were confirmed to be free of mycoplasma and other pathogens using IMPACT II polymerase chain reaction panel testing (IDEXX Bioanalytics, 41–00031).

Humanized PDX

Humanized non–small cell lung cancer (NSCLC) patient-derived xenograft (PDX) tumors were generated by warm-passaging 300 µm × 300 µm × 300 µm PDX LTFs into the hind flank of female NSG mice (The Jackson Laboratory) between 7 and 9 weeks of age. When tumors reached ~50 mm^3, mice were injected intravenously with 10–12 × 10^6 human peripheral blood mononuclear cells from a consenting healthy donor.

Human tissue

Protocols for the collection of human specimens were approved by an institutional review board. Resected tumors were collected by a waiver of consent or informed consent and cold temperature shipped overnight. CNBs were collected under informed patient consent from ongoing clinical trials (ClinicalTrials.gov identifiers: NCT05478538, NCT05520099, NCT06349642) and shipped overnight in NanoCool shipping containers (Peli Biothermal, 2–85225). Data from the shipment of 118 consecutive CNBs showed > 99% of specimens sustained a temperature between −2°C and 10°C for > 98% of the shipping time (Figure S1). For studies including biomarker status, patients were enrolled with colorectal, endometrial, head and neck or lung tumors that have FDA-approved indications for αPD-1 treatment based on companion diagnostic (CDx) biomarkers. At the end of the experiment, IgG-treated LTFs were formalin-fixed, and PD-L1 or MMR protein expression was assessed by immunohistochemical analysis when unavailable from patient records.

Specimen preparation

Tumor resections

Resected tumors were cut into desired dimensions of resection LTFs (eg, length × width × thickness of 300 µm × 300 µm × 300 µm) by a fully automated, proprietary cutting device. To prevent T-cell egress [16], 300 µL of hydrogel (VitroGel-3, TheWell Bioscience) was added to each well of a 24-well plate and mixed with the LTFs by pipetting. Following polymerization, 1 mL of culture media containing the indicated treatment was added to each well.

CNBs

CNBs from 12- to 20-gauge needles were cut into 300-µm slices using an automated, proprietary cutting device. For cross-well comparisons, CNBs were cut perpendicularly (90°) to the longitudinal axis and plated in an 8-well plate, while those for sequential treatment studies were cut at a 20° angle (Figure S2) and plated in a 24-well culture plate. To address the potential for tumor heterogeneity between CNBs, LTFs from CNBs were mixed before plating into assay wells. Hydrogel (VitroGel-3, TheWell Bioscience; or a proprietary formula, Elephas) was added to each well. After hydrogel polymerization, 500 µL of culture media containing the indicated treatment was added to each well.

Treatments

ImmunoCult™ Human CD3/CD28 T-Cell Activator (STEMCELL Technologies Inc, 10971) was used at a final concentration of 25 µL/mL, except in a subset of experiments in which a final concentration of 100 µL/mL was used (see Supplementary Material 1). Immunoglobulin G (IgG) isotype controls and ICI antibodies were used at a concentration of 50 µg/mL (BioXCell). ICI was matched with manufacturer's recommended IgG control, except in 4 specimens (see Supplementary Material 1).

Assays

Viability and cytotoxicity assays

Relative viability was assessed using Cell Counting Kit-8 (CCK8) (Abcam, ab228554). The CCK8 reagent was added immediately after plating, and media were sampled approximately 24 hours later to measure absorbance at 450 nm. Media and reagent were refreshed daily, and the rate of absorbance over time (abs/hour) was calculated. Relative cytotoxicity was measured by the LDH-Glo™ Cytotoxicity Assay kit (Promega, J2381) per manufacturer's instructions.

Optical coherence microscopy imaging

A custom-designed optical coherence microscopy (OCM) system was used as previously described [23] and

fitted with a 15X objective lens (Thorlabs, 0.70 numerical aperture).

Cytokine profiling

Conditioned media collected from individual culture wells at defined time points were assessed using the Human XL Cytokine Luminex Performance Assay Premixed Kit per manufacturer's instructions (R&D Systems, FCSTM18B-30, see Table S1). If the cytokine concentration was above the upper limit of quantitation, the value was set to the upper limit of quantitation. Values below the limit of quantitation were unchanged and removed from analysis where noted. Additionally, 6 analytes (CD40L, EGF, FGF basic, IL-12p70, IL-15, and FLT-3 L) were excluded from analysis due to concentrations consistently falling below the lower limit of quantitation (LLOQ).

Histology

LTFs were fixed in 10% phosphate buffered formalin (Fisher Scientific, SF100-4). Resection LTFs were retrieved from the VitroGel-3 post-fixation and transferred to 70% alcohol before being pre-embedded in a 2% agarose solution (Sigma Aldrich, A0576). CNB LTFs encapsulated in Elephas hydrogel were directly transferred into 70% alcohol post-fixation. Resection and CNB LTFs were paraffin-embedded and sectioned at 5-µm thickness on a rotary microtome (Leica, RM2255) and stained with hematoxylin and eosin (H&E) or processed for immunohistochemistry (IHC) or multiplex immunofluorescence (mIF) using Ventana Medical Systems Discovery Ultra Autostainer (see Table S2 for antibodies used).

Statistical analysis

Data were reported as mean ± standard deviation and statistical significance assessed by Student *t* test or analysis of variance using Prism 10 software (GraphPad) unless otherwise noted. Fisher exact test was performed in the Python SciPy software package [24]. All quantification of histological slides was performed using Visiopharm software. All bar graphs report mean and standard deviation and all violin plots report medians as solid bars with upper and lower broken lines representing the third and first quartiles.

For CNBs following the sequential treatment protocol, ICI-induced change in cytokine concentrations was determined by the fold change (FC) of slope between ICI and IgG control treatment phases (ICI slope/IgG slope).

For resections, ICI-induced change in cytokine concentrations was determined by the difference in cumulative concentrations between ICI- and IgG-treated wells. The median absolute deviation (MAD) values were calculated and any sample within 2 MAD values of the median were then recomputed to generate a trimmed statistic, which was transformed into modified Z-scores (Mod. Z-score) [25].

Agglomerative hierarchical clustering was performed by specimen and analyte using the Ward method in TIBCO Spotfire software. Mod. Z-scores of −10 and 10 were selected as the lower and upper saturation points, respectively. A conservative criterion to identify where upregulation occurred was defined by a Mod. Z-score ≥ 5.0.

Results

Ex vivo platform developed to characterize response to ICIs while addressing challenges associated with tumor heterogeneity in live tumor resections

An ex vivo platform was developed in which live tumor resections were cut into cuboid LTFs using an automated proprietary instrument, pooled randomly and encapsulated in a 3D hydrogel (Fig. 1A). To optimize fragment size and address intra-tumor heterogeneity, in silico simulations were performed on a CD3-stained melanoma cross-section. These simulations showed a significant reduction in the coefficient of variation (CV) of $CD3^+$ T-cell numbers in LTFs with edge lengths of 300 µm ($p < 0.05$) and 100 µm ($p < 0.01$) compared to slices (Fig. 1B–C). Although the lowest CV was observed for the 100-µm edge length, 300-µm LTFs were selected for further characterization given the desire to retain as much contiguous TME as possible without compromising on nutrient diffusion [26]. Therefore, 300-µm cuboid LTFs were generated using an automated cutting instrument producing the expected theoretical surface area of 0.09 mm^2 and a theoretical volume of 0.027 mm^3 across multiple tumor types (Figure S3A-D). These data suggest appropriately controlled cross-well comparisons can be made with pooled LTFs from tumor resections.

To evaluate the effect of LTF number on the variability in measured T-cell response, LTFs from 5 human tumor resections were dispensed at ~50, ~100 and ~200 LTFs per well. Cytokine induction was assessed following 24-hour stimulation with αCD3/αCD28 (positive control for T-cell response). A reduction in variability was observed across most cytokines with increasing LTF number (Figure S4A-B). Additionally, there was a progressive increase in the number of cytokines exceeding LLOQ as LTF count was increased (Fig. 1D). To assess variability in cytokine profiling when using 200 LTFs per well, cytokine concentrations were measured from LTFs derived from 10 human tumor resections following αCD3/αCD28 stimulation (5 replicate wells per tumor). The median CV across all cytokines for each of the individual tumors was below 25% (Figure S4C). A range of variance was observed across individual cytokines, with most cytokines exhibiting an average CV < 20% (Fig.

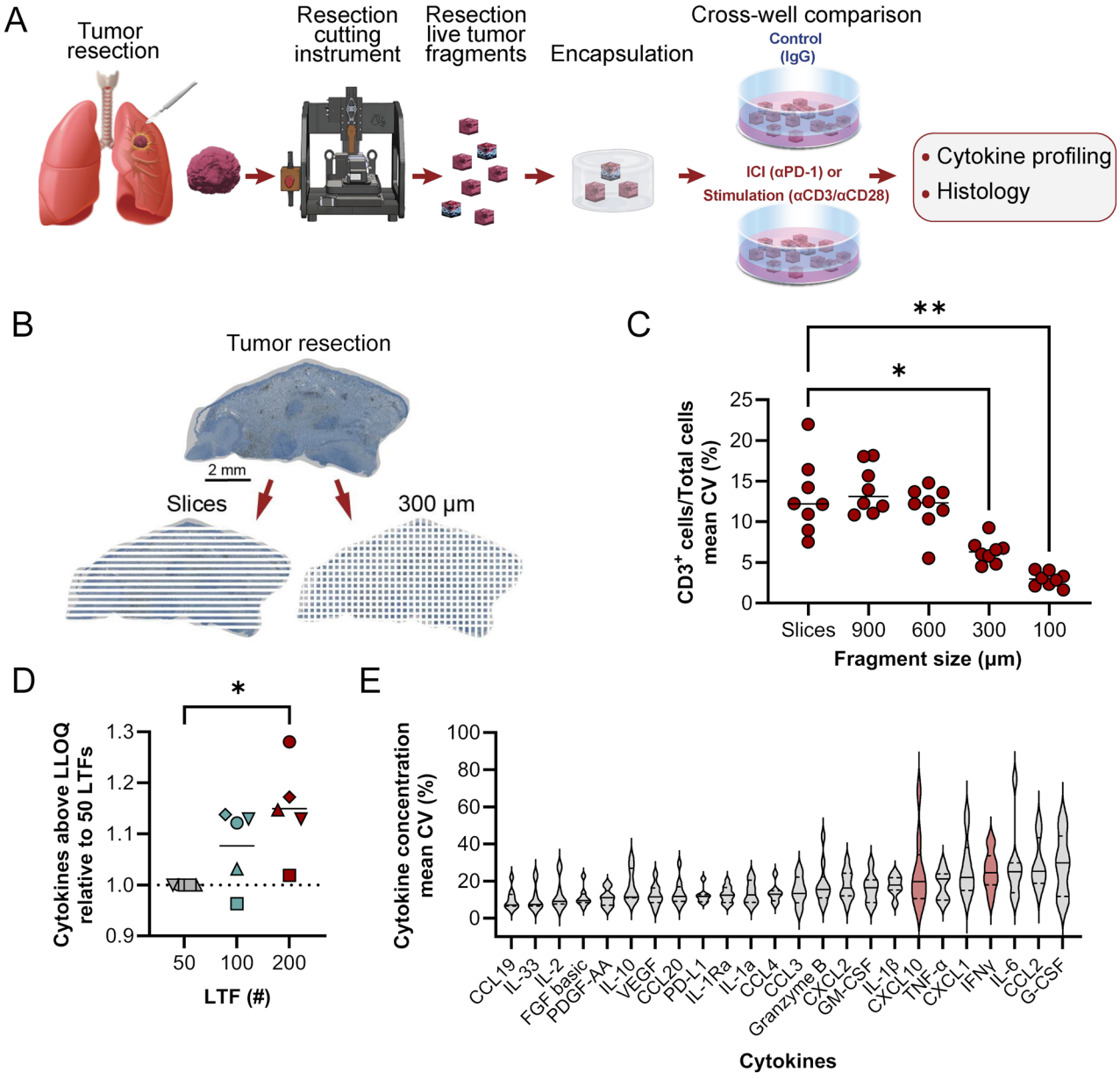

Fig. 1 An ex vivo platform to characterize response to ICIs addresses challenges of tumor heterogeneity. (**A**) Schematic shows the workflow for creating LTFs from human tumor resections used for assessing the ex vivo response to treatment. Tumor resections were fragmented using a specialized cutting instrument to create LTFs, encapsulated in a hydrogel and treated with either an ICI (eg, αPD-1), a positive control for T-cell stimulation (eg, αCD3/αCD28), or IgG control, followed by cytokine profiling to assess response to treatment. (**B**) IHC image of a CD3 stained human melanoma resection showing in silico simulation of a standard slice sampling technique (bottom left) compared with LTF 300 µm x 300 µm segments (bottom right). (**C**) In silico randomized pools of large slices from the melanoma resection showing significantly greater variability in $CD3^+$ staining when compared with randomized pools of LTFs simulating 300-µm edge lengths. (**D**) Effect of LTF number on the percentage of cytokines in the assay panel with measured concentrations exceeding the lower limit of quantitation (LLOQ) following stimulation with αCD3/αCD28 for 24 hours. Data are reported for 5 human tumor specimens (ovarian, n=1, circle; lung, n=1, triangle; colorectal, n=1, upside down triangle; head and neck, n=2, diamond and square). (**E**) Variability (CV [%]) across 5 replicate wells of 200 resection LTFs (300 µm [length] x 300 µm [width] x 300 µm [depth]) from each of 10 human tumors (pancreatic, n=2; head and neck, n=4; ovarian, n=3; triple-negative breast, n=1) stimulated with αCD3/αCD28 for 24 hours. Cytokines of particular interest are CXCL10 and IFNγ (highlighted in red) due to their known roles in T-cell activation. *$p < 0.05$, **$p < 0.005$

1E). This level of variance indicates ~200 LTFs per well enables the detection of > 2-fold changes in cytokine production with statistical significance when paired with multiple replicates.

Tumor microenvironment, tissue viability, and T-cell function of resection LTFs are preserved over 48 hours of ex vivo culture

Cross-section analysis of resected tumors and

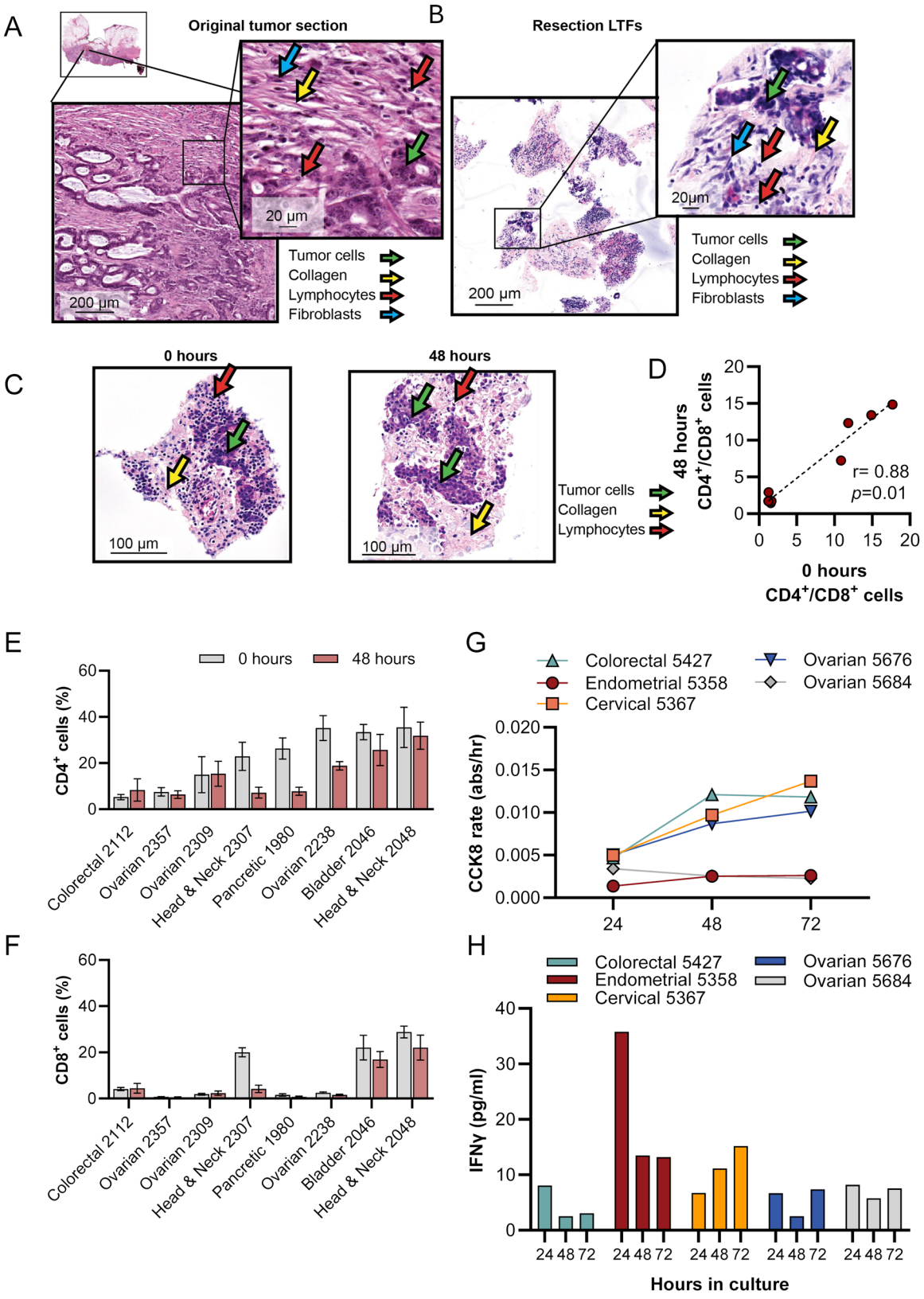

Fig. 2 (See legend on next page.)

(See figure on previous page.)

Fig. 2 Tissue viability and TME are preserved in LTFs over 48 hours of ex vivo culture. H&E-stained sections of a colorectal cancer resection showing low-grade adenocarcinoma. Lymphocytes (red arrows), fibroblasts (blue arrow), tumor cells (green arrow) and collagen fibers (orange arrow) are present in both the intact resection specimen (**A**) and the resection LTFs at 0 hours of culture (**B**). Comparison of H&E images by a board-certified pathologist identified conservation of histology, including intratumor heterogeneity. (**C**) H&E-stained sections of head and neck LTFs at 0 hours and 48 hours of ex vivo culture showing tumor cells (green arrow), collagen fibers (yellow arrow), lymphocytes (red arrow). (**D**-**F**) Comparison of the percentages of $CD4^+$ to $CD8^+$ cell ratios (**D**), $CD4^+$ (**E**), and $CD8^+$ (**F**), at 0 hours vs. 48 hours as assessed by IHC (N=8 human tumors: colorectal, n=1; bladder, n=1; head and neck, n=2; ovarian, n=3; pancreatic, n=1). (**G**) Changes in viability (CCK8 assay) over 72 hours in culture of LTFs derived from 5 human tumor resections. (**H**) Changes in T-cell function over 72 hours of culture in LTFs as assessed by IFNγ production following 24 hours of stimulation with αCD3/αCD28

corresponding LTFs stained with H&E revealed conservation of histological features over 48 hours of culture. The preservation of histological features from the parent tumor was demonstrated by the presence of tumor cells, lymphocytes, fibroblasts, and collagen fibers in both the intact resection specimen (Fig. 2A) and the resection LTFs immediately following fragmentation (Fig. 2B). Resection LTFs encapsulated and cultured for 48 hours ex vivo showed similar histological features to resection LTFs fixed immediately after cutting (Fig. 2C). IHC staining of resection LTFs from 8 tumors representing 5 different tumor types showed reduced total cells ($p < 0.05$, Figure S5A-B), reduced $CD4^+$ cells ($p < 0.05$, Figure S5C) and a trend toward reduced $CD8^+$ cells ($p = 0.07$, Figure S5D) after 48 hours of culture. However, the $CD4^+/CD8^+$ cell ratio was maintained in all tumor specimens (Fig. 2D) with the percentage of $CD4^+$ cells maintained in 5 of 8 tumors (Fig. 2E and S5E) and the percentage of $CD8^+$ cells maintained in 7 of 8 tumors (Fig. 2F and S5F). Taken together, these data suggest the tumor immune microenvironment—particularly the ratio of $CD4^+/CD8^+$ cells—is preserved during ex vivo culture of resection LTFs.

To further assess the preservation of the TME in resection LTFs ex vivo, viability, cell death, and T-cell function were measured in 5 human tumors over 72 hours of culture. Levels of nicotinamide adenine dinucleotide phosphate hydrogen (NAD(P)H), measured using CCK8 [27], served as a proxy for viability [28] while lactate dehydrogenase (LDH) release was used to assess cell death. Figures 2G and S5G show the reciprocal relationship between metabolic activity and cell death over 72 hours in culture. In the first 24 hours, low metabolic rates and relatively high LDH likely reflected damage from tissue processing and/or acclimation to culture conditions. Subsequent time points showed steady or slight increases in metabolic activity and corresponding steady or slight decreases in cell death. This trend continued through 72 hours, demonstrating the culture conditions support cell viability. To assess whether T cells were stimulable, and therefore functional, resection LTFs were stimulated with αCD3/αCD28 at either 0, 24, or 48 hours, and then assayed for interferon gamma (IFNγ) production 24 hours later. Similar IFNγ levels were observed when resection LTFs were stimulated 24 or 48 hours from the start of culture, suggesting T cells are viable ex vivo for at least 72 hours (Fig. 2H). Reduced IFNγ production in LTFs stimulated at 24 hours compared with those stimulated at 0 hour is consistent with the decrease in the $CD4^+$ and $CD8^+$ cell populations seen histologically in some samples (Figures S5C-F), as has been observed by others [29].

Unsupervised hierarchical clustering groups PD-L1/MMR/MSI biomarker-positive samples amongst those with the greatest cytokine upregulation following ICI treatment

To demonstrate cutting and randomized pooling of LTFs sufficiently addresses intra-tumor heterogeneity and therefore allows for a properly controlled comparison between control and αPD-1 treatments, response to αPD-1 was assessed using LTFs generated from 59 human resections (Table S3, Figure S6A). Clustering of normalized differences in cytokine concentrations (αPD-1 - IgG) revealed groups of tumors with little to no cytokine upregulation (lower Z-scores) in response to ICI on the left and groups of tumors with upregulated cytokines in response to ICI on the right (higher Z-scores) (Fig. 3A and S6B). This result suggests increased cytokine production in response to ICI treatment is observed in a subset of tumor specimens.

Next, the relationship between ICI-induced cytokine changes and CDx biomarker status (eg, expression of PD-L1 or MMR proteins, or levels of MSI) was evaluated. A significant enrichment in cytokine upregulation was observed in the PD-L1/MMR/MSI-positive (PD-L1+/dMMR/MSI-high) population compared to the PD-L1/MMR/MSI-negative (PD-L1-/proficient mismatch repair [pMMR]/not MSI-High) population (Fig. 3B). Further analysis of individual T-cell response cytokines showed significant enrichment of IFNγ and C-X-C motif chemokine ligand 10 (CXCL10) upregulation (higher Z-scores) in the biomarker-positive samples compared with the biomarker-negative samples (Figs 3C-D and Table S4). These data suggest that automated tissue fragmentation and randomized pooling of resection LTFs address tumor heterogeneity and may allow one to effectively model ICI treatment response in human tumor resections.

CNBs with limited tissue availability are less amenable to fragment-pooling approach to overcome tissue heterogeneity

Multiple replicates of control and treated wells enable meaningful cross-well comparisons when sufficient

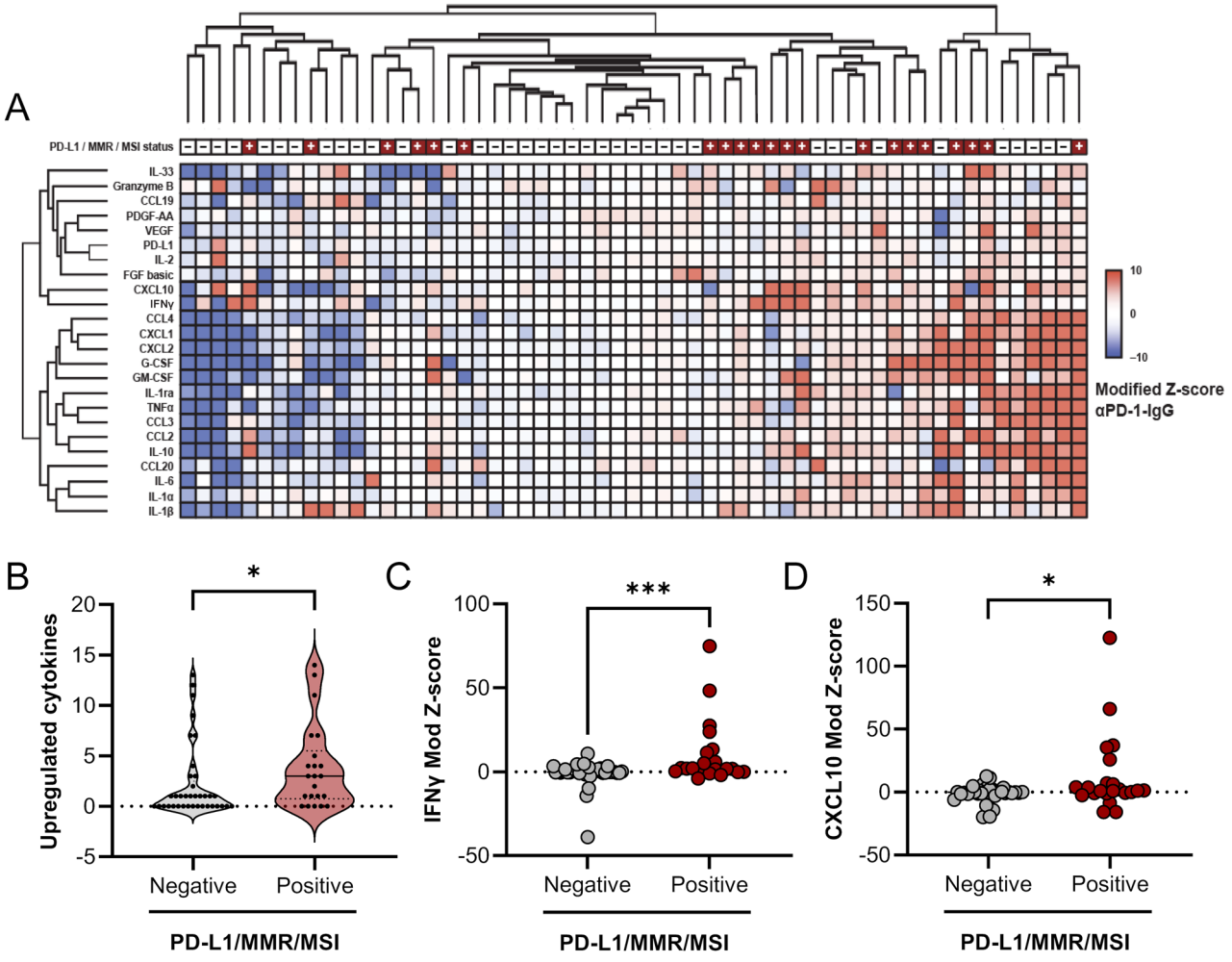

Fig. 3 Unsupervised clustering groups PD-L1/MMR/MSI-positive specimens amongst those with the greatest cytokine upregulation following ICI treatment. (**A**) Unsupervised hierarchical clustering of cytokine profiles from patient tumor resections using modified Z-scores of the difference in cytokine concentrations between the ICI- and IgG-treated groups. To account for variability across wells, replicate wells for each treatment group were run for those specimens where sufficient tissue was available (n=3 for 48 specimens, n=2 for 6 specimens, and n=1 for 5 specimens). Positive modified Z-scores (capped at 10) are depicted in shades of red and negative modified Z-scores (capped at -10) are depicted in shades of blue. Specimens with Z-scores of 0 are depicted in white. PD-L1/MMR/MSI-positive specimens are annotated in red at the top of the heatmap; *N*=59 specimens. (**B**) The number of upregulated cytokines for individual specimens, defined by a modified Z-score ≥ 5, is significantly higher in the PD-L1/MMR/MSI- positive cohort compared with the PD-L1/MMR/MSI-negative cohort. Two cytokines known to be associated with T-cell activation, IFNγ (**C**) and CXCL10 (**D**), are significantly increased in PD-L1/MMR/MSI-positive compared with PD-L1/MMR/MSI-negative cohorts. *$p < 0.05$, ***$p < 0.001$

tissue is available, addressing heterogeneity in tumor resections. However, CNBs, used in standard practice during clinical diagnosis, pose a challenge due to the scarcity of tissue available to address intra-tumor heterogeneity, making conventional cross-well comparison requiring multiple replicates less feasible (Fig. 4). To confirm this, we compared control (IgG) and treated (αPD-1) cytokine concentrations between pooled LTFs from 59 human tumor resections with pooled LTFs from 24 CNB specimens in a cross-well manner. To assay multiple wells from a single CNB specimen, CNBs were cut at a 90° angle to maximize the number of CNB LTFs obtained (Table S5). As a result, 3–5 CNB LTFs were plated per well, with triplicate wells prepared for each condition. The media amount per well was reduced to maintain a tissue-to-media volume ratio consistent with that used in resection LTF experiments. While the number of quantifiable cytokines in the tumor resections was similar to those from the CNB specimens for IgG controls (Fig. 4B), there was significantly greater variation in ICI-induced cytokine production in the LTFs from CNB tumors compared with resection tumors (Fig. 4C, Figure S7), suggesting heterogeneity was not fully addressed in pooled LTFs from CNBs. The limited amount of tissue from a single CNB (eg, an 18 gauge of ~10 mm in length) is roughly equivalent to the tissue amount used in a single well of 200 resection LTFs (total tissue volume about 5.4 mm^3) and cannot support the 6 replicate wells that would be

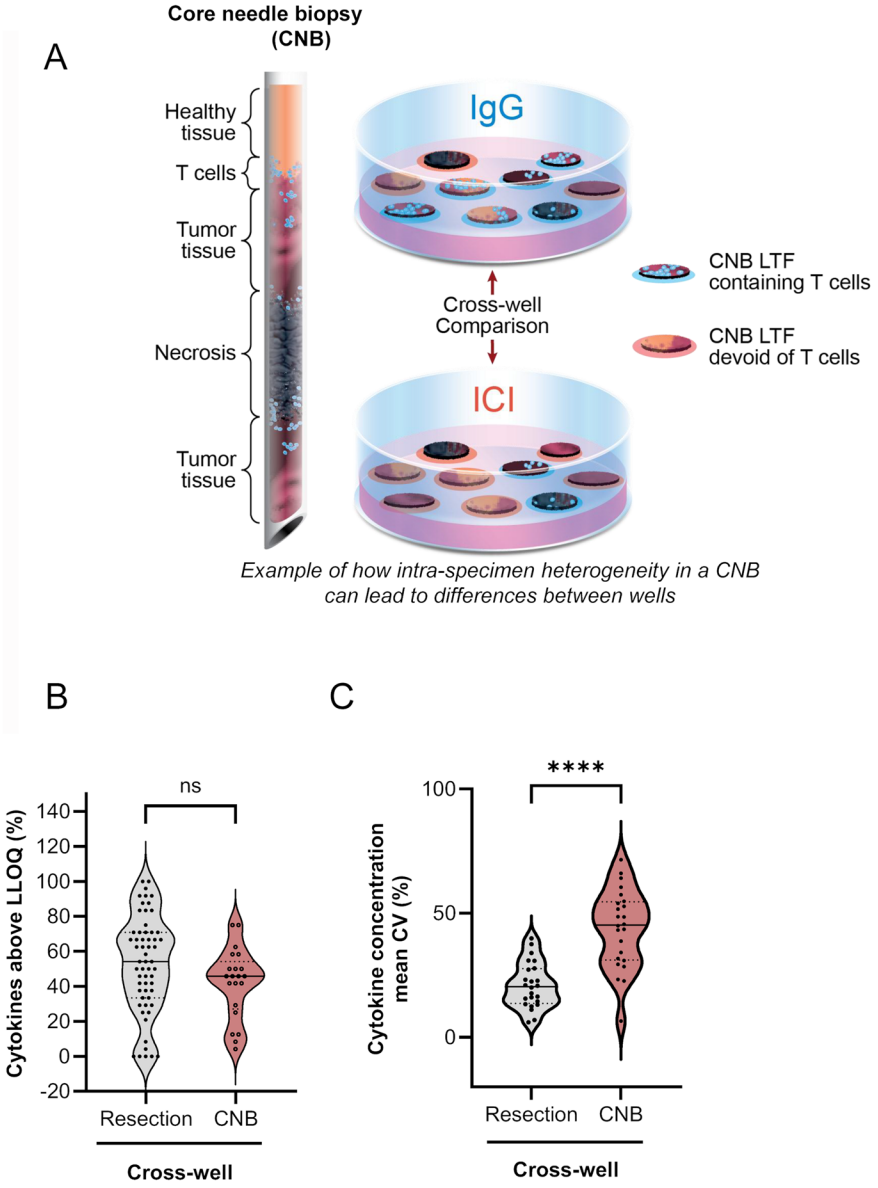

Fig. 4 CNBs, with limited tissue amount, are not amenable to cross-well measurement of cytokine response to ICI. (**A**) Schematic showing the distribution of tissue from a CNB in an experiment using the cross-well configuration where tissue amount is insufficient to address intra-specimen heterogeneity. (**B**) The percentage of cytokines out of a 30-cytokine panel with concentrations above LLOQ for the cross-well configuration for human resection LTFs (resection cross-well) and human CNB LTFs (CNB cross-well) following treatment with IgG control for 24 hours. There is no significant difference in the ability to detect cytokines between the two form factor protocols (ns = not significant, $p = 0.089$). (**C**) The variability in concentrations of cytokines from resection LTFs and CNB LTFs plated in the cross-well configuration and treated with ICI for 24 hours. There is significantly greater variability in cytokine concentrations between replicate wells of treated groups in CNB LTFs compared with resection LTFs. **** $p < 0.0001$

needed for a meaningful cross-well comparison as shown using resection LTFs reported in Fig. 3. These results suggest intra-specimen heterogeneity is not mitigated in pooled CNB LTFs, and tissue scarcity does not allow for a robust cross-well comparison between control and treatment regimens.

Challenges associated with tumor heterogeneity in CNBs can be addressed using a sequential treatment strategy

To address tumor heterogeneity and the compounding tissue scarcity of CNBs, a sequential treatment strategy was devised wherein CNB LTFs were treated sequentially with the negative control followed by ICI within the same well. The treatment effect was evaluated via longitudinal assessment of cytokine production rates. Here, the tissue was stimulated after a control phase in the sequential treatment setting to determine whether

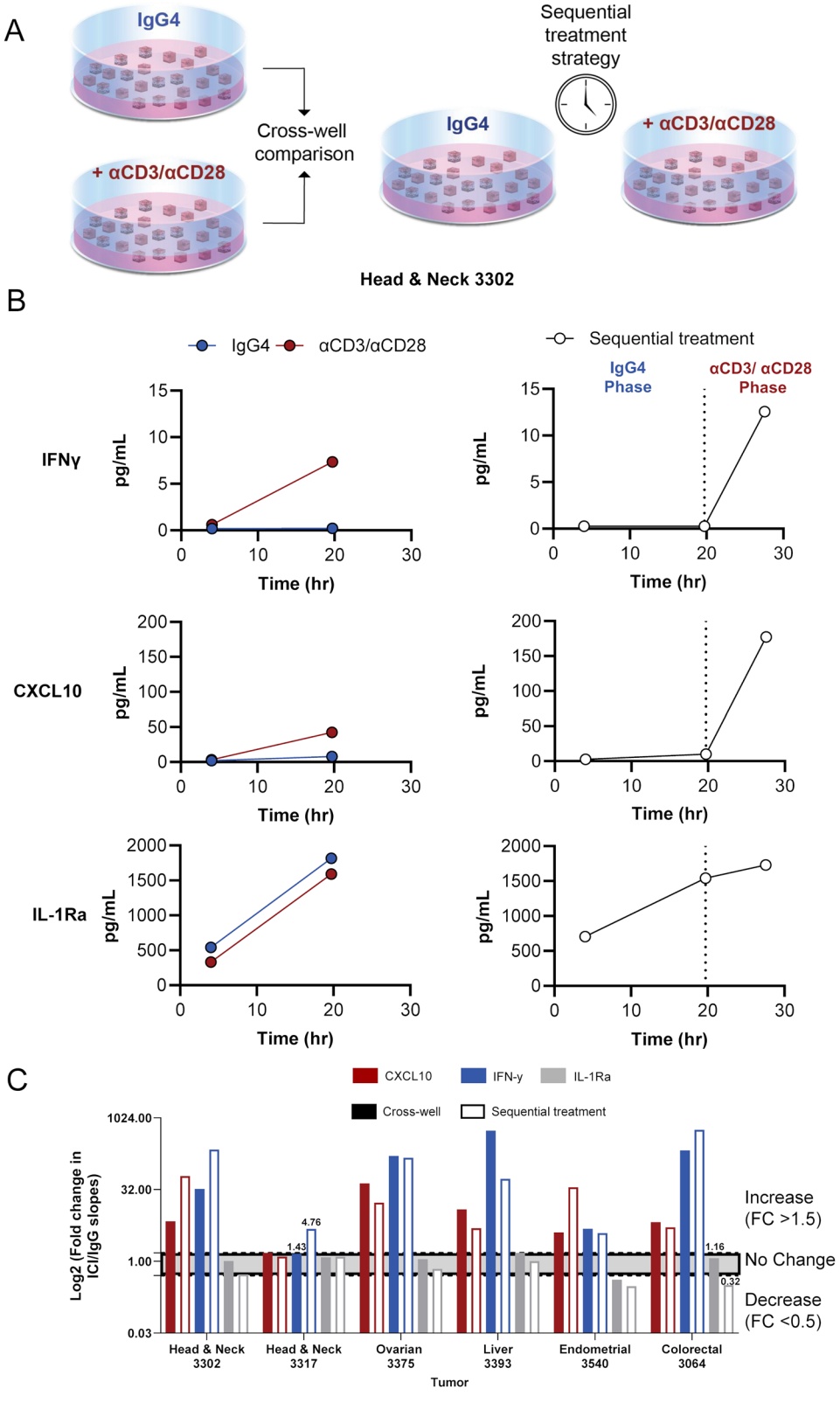

Fig. 5 (See legend on next page.)

(See figure on previous page.)

Fig. 5 Challenges associated with intra-specimen heterogeneity can be addressed using a sequential treatment strategy. **(A)** Schematic of the protocol used to validate sequential treatment strategy. Human tumor resections were used due to the availability of sufficient tissue to address inter-well heterogeneity in tissue composition and enable meaningful cross-well comparisons. Tumor resections were cut into resection LTFs, encapsulated in hydrogel and treated with IgG4 for 20 hours (shown in blue), positive control αCD3/αCD28 to stimulate T cells for 20 hours (shown in red), or IgG4 for the first 20 hours and αCD3/αCD28 for the final 8 hours of culture (shown in red). Conditioned media were sampled from each of the wells at 4, 20, and 28 hours for cytokine profiling. (**B**) IFNγ and CXCL10 induction in a head and neck human tumor specimen was observed following αCD3/αCD28 stimulation in cross-well (left) and sequential treatment (right). IL-1Ra remained unchanged following αCD3/αCD28 stimulation. (**C**) To characterize the similarity in cytokine production following the cross-well and sequential treatment experimental designs, the FC in rates (slopes) of cytokine production following αCD3/αCD28 stimulation were calculated compared with rates of cytokine production during IgG4 exposure. The FC in rates of cytokine production for cross-well and sequential treatment strategies were compared to determine similarities of magnitude and direction (increase >1.5; no change = 0.5-1.5; decrease <0.5). IFNγ, CXCL10, and IL-1Ra showed 83%, 100%, and 83% concordance, respectively, between cross-well and sequential treatment strategies. Numerical labels are shown in cases of discordant cross-well and sequential treatment data. Grey band indicates no change

it elicited a response similar with stimulating immediately after encapsulation. For these experiments, 300 µm resection LTFs at a target of 200 LTFs per well were used to address intra-specimen heterogeneity and enable a meaningful comparison between conditions in a cross-well setting. Resection LTFs were either treated within dedicated wells for 28 hours with IgG4 or αCD3/αCD28 (cross-well), or within the same well for 20 hours with IgG followed by αCD3/αCD28 for an additional 8 hours (sequential treatment) (Fig. 5A). Longitudinal, cumulative concentration assessment of CXCL10 and IFNγ from a representative human head and neck tumor resection showed an increased production rate with αCD3/αCD28 stimulation for both cross-well and sequential treatment experiments (Fig. 5B). Inclusion of 5 additional tumors showed a similar trend with 100% concordance between cross-well and sequential treatment with increases in the slopes of IFNγ and CXCL10, in response to αCD3/αCD28 treatment over IgG. While the magnitude of increase in IFNγ and CXCL10 in response to αCD3/αCD28 between cross-well and sequential treatment varied, the directionality of response was in high agreement with 5 of 6 tumor samples showing concordance for IFNγ and 6 of 6 for CXCL10 as measured using a > 1.5-fold change as an indicator of increased rate of cytokine production (Fig. 5C). Additionally, interleukin-1 receptor agonist (IL-1Ra), a regulatory cytokine, was well expressed at baseline and did not change significantly following αCD3/αCD28 treatment. For this reason, IL-1Ra is used to highlight a ubiquitously expressed, non-responding cytokine in the analysis.

Longitudinal imaging is enabled with CNB LTFs when using a specialized cutting instrument and encapsulation in a proprietary hydrogel

Leveraging the advantages of the sequential treatment strategy, which does not require multiple wells, LTF generation was adapted, shifting from creating cuboid LTFs optimized for efficient randomization to producing larger LTFs with a greater area of contiguous tissue architecture that allows for better assessment of spatial tissue organization and cell interactions (Fig. 6A).

Assessment of cellular features and interactions in cultured tissue over time by imaging requires the ability to register tissue loci easily for repeated longitudinal assessment. To reduce fragment movement, a proprietary hydrogel (Elephas hydrogel) was designed and tested against a commercially available hydrogel (VitroGel-3). CNB LTFs generated from a CT26 syngeneic mouse tumor were encapsulated in either VitroGel-3 or Elephas hydrogel and cultured for 72 hours (Fig. 6B). The positions of LTFs were tracked over time and the magnitude of movement was quantified for the 2 hydrogels. CNB LTFs encapsulated in the commercial hydrogel showed significant drift over time in culture while CNB LTFs encapsulated in Elephas hydrogel were stable (Fig. 6C). Dynamic optical coherence microscopy (dOCM), which enables measurement of intra-cellular activity (eg, mitochondrial movement), was employed to longitudinally evaluate viability through measuring metabolic activity of LTFs from 3 human CNBs over a 48-hour period. Representative dOCM images from 0 hours and 48 hours, where viable/metabolically active tissue (Viable, false-colored in green) and metabolically inactive tissue (Non-metabolically active, false-colored in magenta) were visualized (Figs. 6D–6E). Over the course of culture, the tissue-maintained viability with a similar proportion of viable tissue area between 0 and 48 hours (Fig. 6F). Quantitative analysis of the 6 individual CNB LTFs from the same NSCLC specimen further supports this trend by showing the maintenance of viable tissue over 48 hours in culture (Fig. 6G). The variation in viable tissue proportions in these CNB LTFs at hour 0 highlights CNB heterogeneity. These findings support the compatibility of the platform with dOCM as a non-invasive technique to track metabolic changes in viable tissue over time.

CNB LTFs encapsulated in Elephas hydrogel retain cellular components of the TME over 48 hours of ex vivo culture

To demonstrate that Elephas hydrogel retains T cells within CNB LTFs, IHC staining was performed to identify $CD3^+$ T cells in un-encapsulated and encapsulated CNB LTFs from humanized PDX tumors after 48 hours of ex vivo culture (Fig. 6H). The proportion of $CD3^+$ T

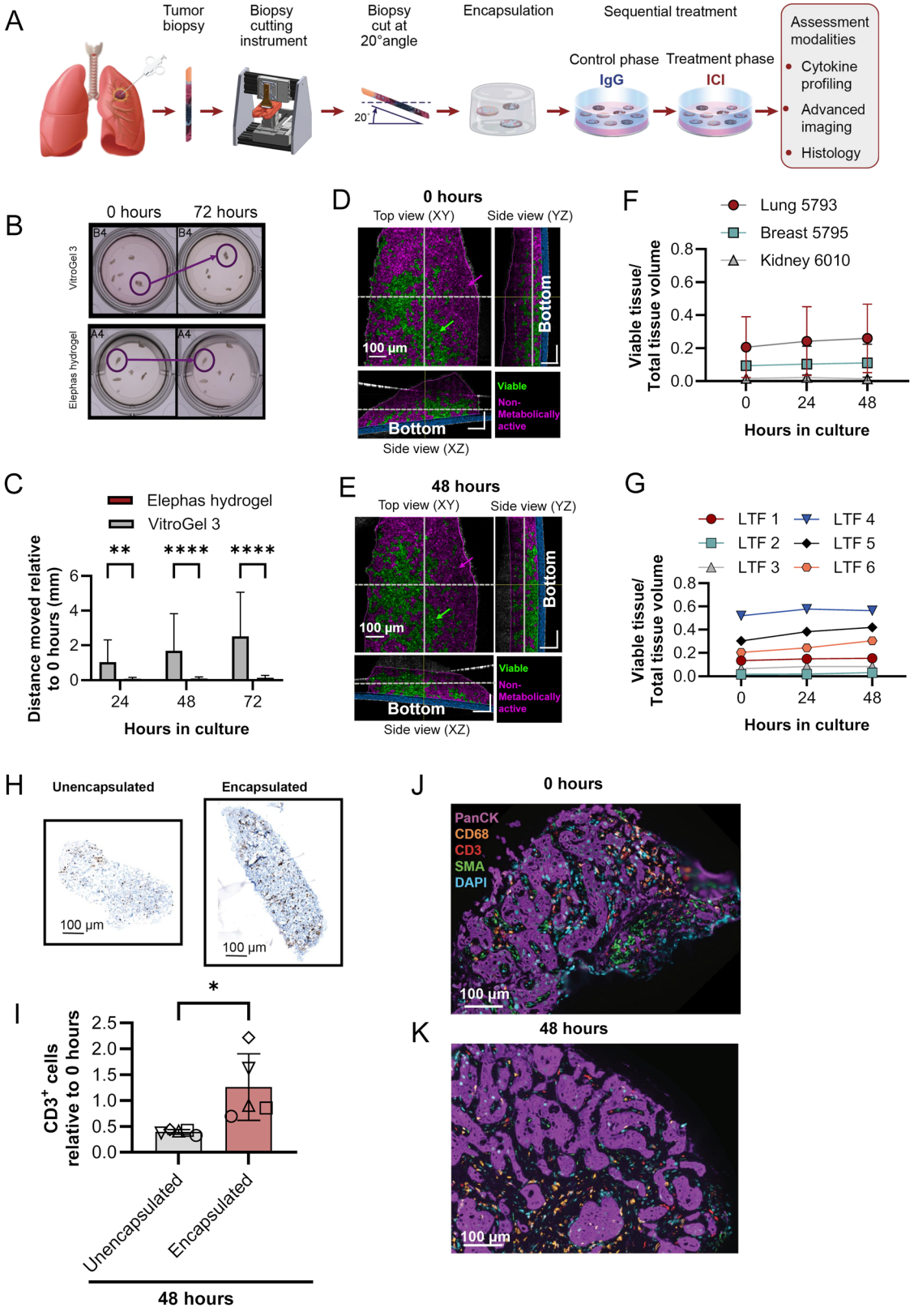

Fig. 6 (See legend on next page.)

(See figure on previous page.)

Fig. 6 The ex vivo platform enables longitudinal advanced imaging and retains T cells in LTFs. (**A**) Schematic shows the workflow for creating LTFs from CNBs used for assessing ex vivo response to treatment. CNBs are sliced at 20° using a specialized cutting instrument to create LTFs which are encapsulated in a proprietary hydrogel (Elephas hydrogel) for ex vivo culture, enabling cytokine profiling, histology, and advanced imaging. (**B**) The spatial stability of LTFs created from CT26 tumors (N=4) over 48 hours of culture when encapsulated in VitroGel-3 versus Elephas hydrogel. Circles highlight regions where LTF stability is compromised with VitroGel-3 but not Elephas hydrogel. (**C**) Distances between CNB LTF locations at 72 hours vs 4 hours of culture. Improved stability was observed with Elephas hydrogel, enabling longitudinal advanced imaging. (**D-E**) dOCM images of a human lung CNB LTF at 4 hours (**D**) and 48 hours (**E**) in culture. Volume positive for metabolic activity is false-colored green and volume negative for metabolic activity is false-colored magenta. (**F**) Ratios of viable voxels to total voxels are reported across 3 human tumors (lung, breast, kidney) showing maintenance of viability over 48 hours in culture. (**G**) The ratio of viable volume to total volume reported for 6 CNB LTFs from Lung 5793 highlights heterogeneity in viability across LTFs from one CNB. (**H**) Representative CD3-stained sections of humanized PDX CNB LTFs from unencapsulated (left) and encapsulated (right) tissues after 48 hours of culture. (**I**) A significant decrease in the number of $CD3^+$ cells, normalized to area, is seen in unencapsulated versus encapsulated LTFs after 48 hours in culture (each symbol represents 1 tumor, N=5 tumors per group, *p < 0.05). (**J-K**) Multiplex immunofluorescence labeled fragments from Liver 5605 show the presence of tumor cells (PanCK), macrophages (CD68), T cells (CD3), stroma/fibroblasts (SMA) and cell nuclei (DAPI) at 0 hours (**J**) and 48 hours (**K**) in culture

cells retained within CNB LTFs after 48 hours in culture relative to 0 hours was significantly higher in encapsulated CNB LTFs than unencapsulated LTFs ($p < 0.05$, Fig. 6I).

Similar to resection LTFs, a steady or increasing rate of viability as assessed by CCK8 over 72 hours of culture (Figure S8A) and a concurrent steady or decreasing rate of LDH accumulation following an initial spike within the first 24 hours (Figure S8B) were observed in data from 4 human tumor specimens. Assessment of CNB LTFs by H&E staining showed retention of major histological features between 0 and 48 hours in culture (Figure S8C), similar to the preservation in resection LTFs observed earlier (Fig. 2C). In addition, mIF confirmed the preservation of cellular composition in LTFs, including T cells, macrophages, tumor cells and fibroblasts (Fig. 6J-K). Together, the retention of histological features as well as the results from metabolic and cytotoxicity assays suggest the overall viability of CNB LTFs is maintained throughout ex vivo culture similar to what was observed in cuboid LTFs from resections (Fig. 2). Changing the form factor from 300-µm cuboid LTFs to larger elliptical slices did not have an appreciable effect on the ability to culture and maintain the TME.

The sequential treatment strategy allows for characterization of ICI response ex vivo in CNBs

The efficacy of the sequential treatment strategy was determined in diagnostic CNBs obtained from an initial set of 16 patients enrolled in 3 ongoing clinical trials. After CNBs were sliced on a proprietary cutting instrument, LTFs were plated, encapsulated, and cultured for 48 hours to assess cytokine response to ICI treatment. LTFs were treated with IgG at the start of culture and then with αPD-1 (lung specimens), anti-programmed cell death 1 ligand-1 (αPD-L1; gastrointestinal specimens), or αPD-1 + αCTLA-4 (kidney specimens) at around 20 hours, such that LTFs in each well received control and ICI treatment sequentially (Fig. 7A). Variable cytokine response profiles across specimens were observed. For example, in Lung 4624, Colon 4834, and Kidney 5023 there was an increase in the rate of accumulation (slope) of both IFNγ and CXCL10 during ICI treatment, relative to IgG control (Figs. 7B, 6E, and 7H, top and bottom, respectively). Conversely, in Lung 4578, Esophageal 4798, and Kidney 5327 the rates of accumulation (slope) of both IFNγ and CXCL10 remained unchanged during ICI treatment relative to control (IgG) (Figs. 7C, 7F, and 7I, top and bottom, respectively). In contrast to the robust increases observed with T-cell response cytokines IFNγ (max FC = 12.4) and CXCL10 (max FC = 19.2), IL-1Ra showed a limited change in slopes between the treatment and control phases (max FC = 3.9; Fig. 7D, G, and J, and Figure S9A-F), suggesting specific changes in immune related cytokines can be measured using the sequential treatment approach following treatment with ICI.

Clinical response in a patient with NSCLC who also had a cytokine response to αPD-1 treatment

To compare platform response with clinical response, clinical records were reviewed to determine which of the 16 patients mentioned in the previous section were treated with a regimen containing immunotherapy and also presented with an objective response to that treatment (tumor reduction > 30%, as measured by Response Evaluation Criteria in Solid Tumors [RECISTv1.1]). Of these 16 patients, one met both criteria (NSCLC patient 4624 with stage IV lung adenocarcinoma) who showed a partial response at 3 months following a regimen of pembrolizumab, carboplatin, and pemetrexed. While the clinical response can be attributed to either the immunotherapy, chemotherapy, or their combination, platform response suggests this patient would indeed have a response to αPD-1. Cytokine responses were assessed across 6 replicate wells from 4 provided CNBs (Fig. 8A).

Histological analyses, including H&E and multiplex mIF, revealed the presence of a tertiary lymphoid structure in a biopsy LTF from a replicate well that exhibited increased cytokine response (Note star data point in Fig. 8A and example images in Fig. 8B–D). The patient was subsequently treated with pembrolizumab in combination with pemetrexed and carboplatin. Comparison

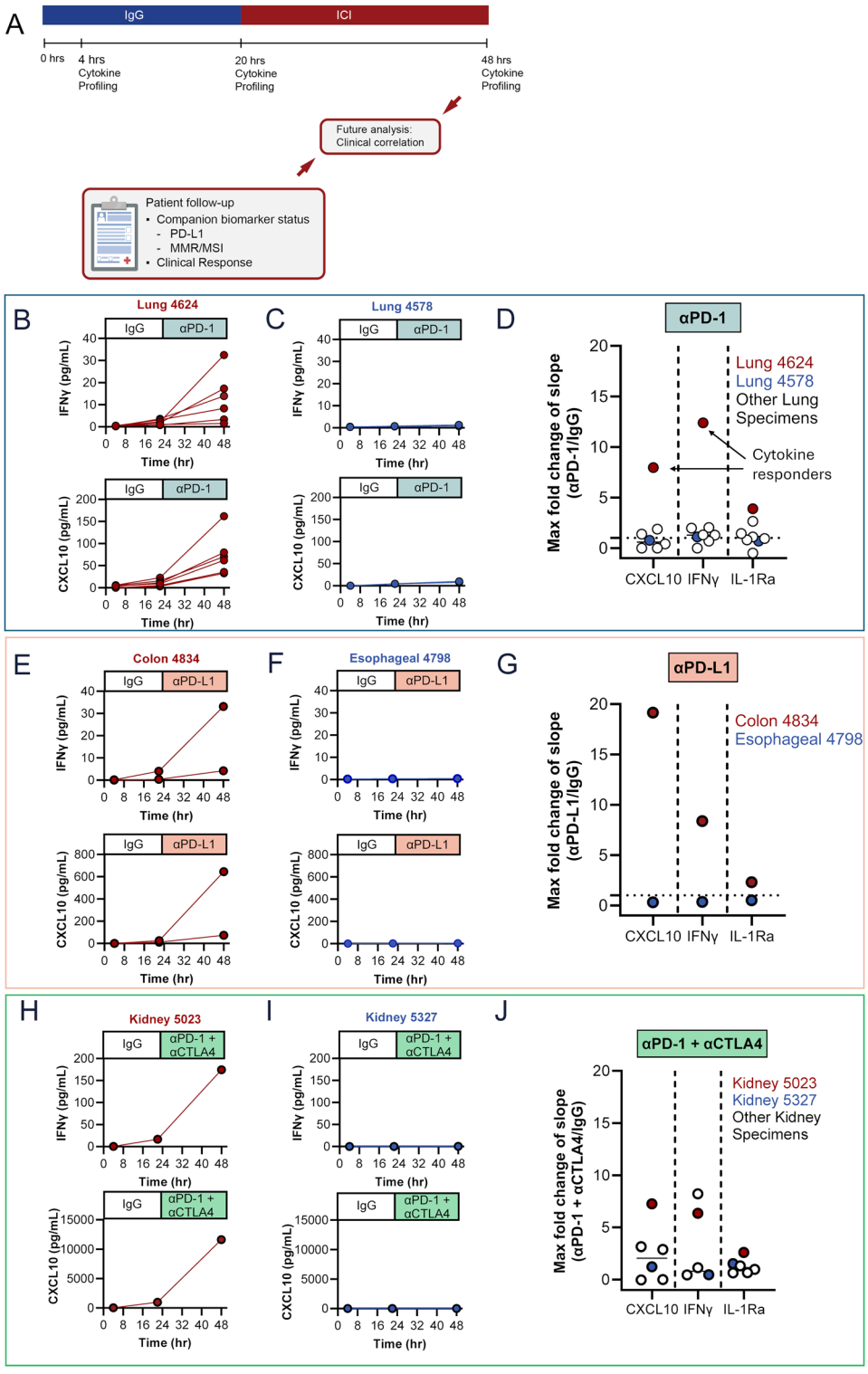

Fig. 7 (See legend on next page.)

of baseline (Fig. 8E) and 3-month (Fig. 8F) computed tomography scans showed a 37% reduction in tumor size and a partial response per RECIST1.1 criteria. This outcome illustrates the potential for utilizing ex vivo cytokine response to guide ICI treatment in the clinic.

(See figure on previous page.)

Fig. 7 A sequential treatment strategy allows for characterization of ICI response in CNBs ex vivo. (**A**) Encapsulated LTFs from CNBs are sequentially treated with IgG control followed by ICI. Conditioned media are collected at the ~4-, ~20- and ~48-hour time points to enable measurement of cytokine concentrations which are used to calculate the rate of cumulative cytokine production during the control (4–20 hours) and ICI (20–48 hours) treatment phases. FC in the rate of cytokine production (slope of ICI treatment phase/slope of IgG control phase) can be used to assess ex vivo treatment response. Exemplary human lung (**B**, lung 4624 treated with αPD-1), colon (**E**, colon 4834 treated with αPD-L1) and kidney (H, kidney 5023 treated with αPD-1 + αCTLA-4) cancer CNBs exhibiting an increase in rate of IFNγ and CXCL10 production following ICI treatment suggesting a potential cytokine response. Exemplary human lung (**C**, lung 4578 treated with αPD-1), esophageal (**F**, esophageal 4798 treated with αPD-L1) and kidney (**H**, kidney 5327 treated with αPD-1 + αCTLA-4) cancer CNBs exhibiting a similar rate of IFNγ and CXCL10 production between the ICI and IgG treatment phases suggesting an unlikely cytokine response. Note that multiple CNBs were obtained from patients 4624, 4578 and 4834 enabling profiling of replicate wells. The FC in the slope of the ICI treatment phase compared to the slope in the IgG treatment phase for IFNγ and CXCL10 across 7 lung (**D**), 2 gastrointestinal (**G**) and 6 kidney (**J**) cancer CNBs. Individual data points report maximum FC for those specimens where multiple CNBs/replicate wells were profiled. Note that the maximum FC for the exemplary cytokine responsive specimens (lung 4624, colon 4834 and kidney 5023, shown in red) is at the top of the distribution while the maximum FC for the exemplary cytokine nonresponsive specimen (lung 4578, esophageal 4798 and kidney 5327, shown in blue) is close to 1

Discussion

The ex vivo platform described here enables characterization of cytokine response to ICIs while addressing the challenges of tumor heterogeneity and limited tissue availability in clinically relevant CNBs. By preserving the native TME, this approach maintains the architectural and cellular context essential for an accurate assessment of immune response. The sequential treatment strategy, wherein CNB LTFs are exposed to a control followed by ICI in the same well, enables paired comparisons within individual replicates. This design mitigates sampling bias, maximizes tissue usage, and facilitates assessment of ICI-induced cytokine induction in a short timeframe, even in biopsies with limited tissue availability.

An intact TME is increasingly recognized as being crucial for assessing ICI response ex vivo, due to the complex interactions among its diverse cell types that influence treatment outcomes. Components of the TME, such as cancer-associated fibroblasts [30], tumor-associated macrophages [31], T cells [32] and the tumor cells themselves [33], have been shown to be intricately involved in orchestrating ICI response. Furthermore, the spatial organization and interactions of these cells within the TME are crucial for effective immune responses and subsequent ICI efficacy [34–36]. Resection and CNB LTFs preserve the native TME, retaining histological features such as fibroblasts, tumor cells, and immune cells—including T cells and macrophages—through the end of the culture period. T cells retained in LTFs encapsulated with the Elephas hydrogel remain responsive to stimulation, allowing for the serial assessment of cytokine induction rates following ICI treatment. More importantly, T cells are exposed to ICI treatment within the context of the native TME in large contiguous sections of tumor tissue, thus preserving the complex spatial relationships that influence treatment efficacy.

Representation of tumor heterogeneity is both critical for accurate prediction of response to immunotherapy and problematic to cross-well experimentation through the introduction of variation resulting from tumor sampling. It is therefore important to represent the heterogeneity of tumors, while reducing the potential for high variance, which can confound the measurement of treatment effects. To address this, the resection-based protocol generates randomized pools of cuboid LTFs to support cross-well cytokine comparisons. However, cytokines known to be induced by immune cell activation, such as IFNγ and CXCL10, show higher variances, likely a result of the differential distribution of T cells and other immune cells across tissue. This necessitates the use of multiple replicates for robust statistical evaluation. The platform's ability to maintain tumor heterogeneity and the native TME was demonstrated in human tumor resections, where ICI-induced cytokine responses were associated with PD-L1 and MMR/MSI status. A perfect alignment of upregulated cytokine clustering among biomarker-positive tumors was not observed, as expected given the imperfect accuracy of current biomarkers (2–7). Future studies assessing the correlation between ex vivo and clinical responses will determine whether the platform can better predict response to ICI therapy.

Preliminary experiments with CNBs from lung, kidney, and gastrointestinal tumors revealed cytokine induction patterns unique to individual specimens, particularly in IFNγ and CXCL10. In cases where CNB tissue amount supported multiple replicates for assessment, intra-specimen heterogeneity was evident from the range of observed responses to ICI treatment. However, the sequential treatment approach allows for assessment of response within each individual replicate such that a positive response in any replicate suggests potential treatment sensitivity, while the absence of response across all replicates indicates potential resistance. The preliminary clinical trial results from a patient with NSCLC illustrate the predictive potential for this platform. However, the patient received αPD-1 therapy in combination with chemotherapy, confounding interpretation of the observed clinical response as it is unclear which therapy or the combination was responsible for the clinical efficacy. Ongoing collection of additional clinical trial data from patients treated with ICI monotherapy will help to provide unambiguous validation of the platform.

While this platform offers significant advantages, some challenges warrant mention. First, necrotic biopsy

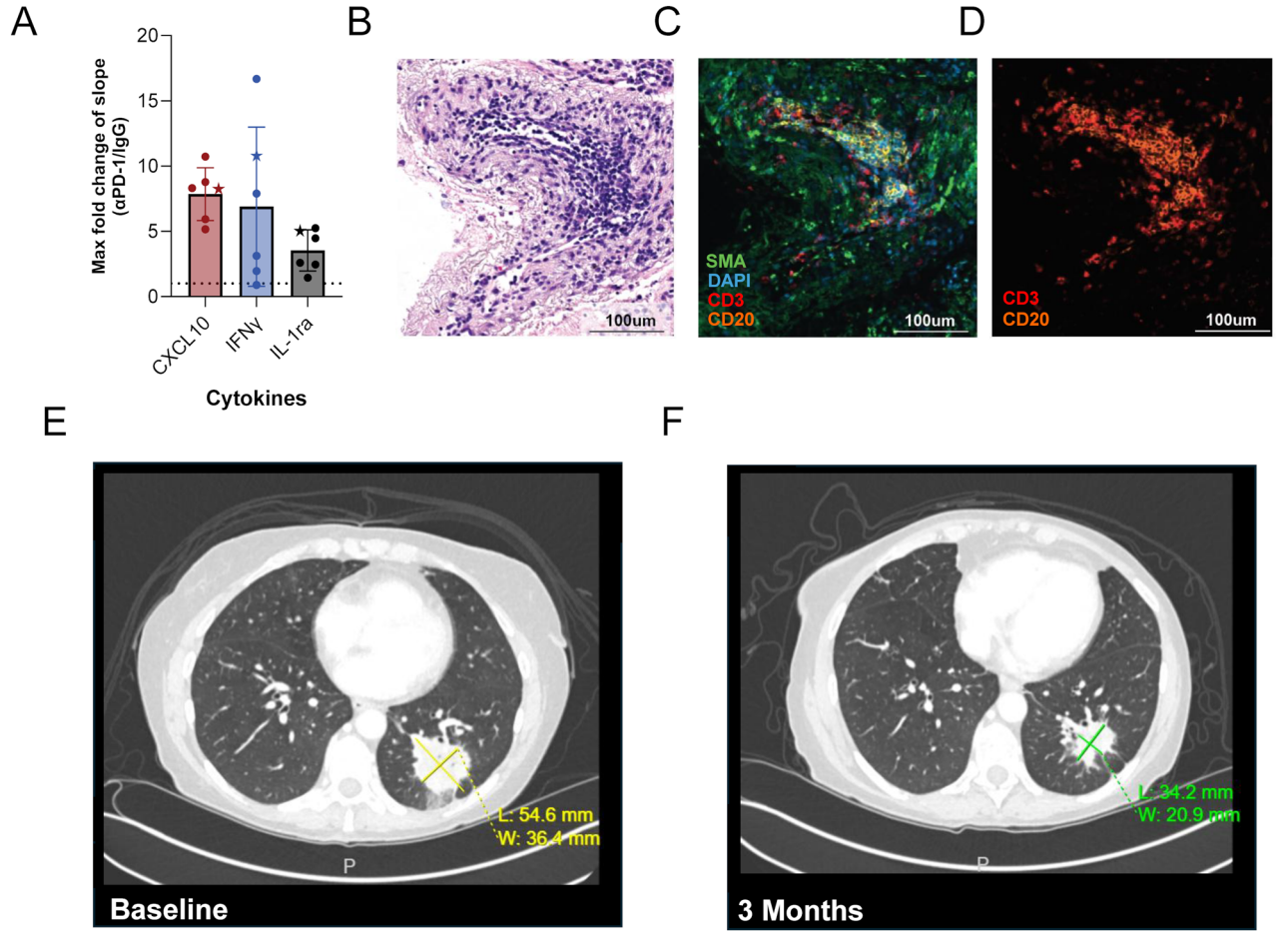

Fig. 8 Clinical response in a patient with NSCLC who had a cytokine response to αPD-1 treatment. (**A**) The FC of the slope in the αPD-1 treatment phase compared with the slope in the IgG treatment phase for IFNγ, CXCL10, and IL-1Ra across 6 replicates (N=4 CNBs) from a single NSCLC tumor specimen. Each symbol represents a unique replicate, with the star indicating the sample well used for histology. H&E- (**B**) and mIF-labeled images (**C**) show the presence of B cells (CD20), T cells (CD3), stroma/fibroblasts (SMA) and cell nuclei (DAPI) from one of the replicate wells assessed ex vivo, highlighting the formation of a tertiary lymphoid structure. (**D**) Shows the independent channels for CD3 and CD20 shown in (**C**). Clinical computed tomography scans show a 37% reduction in the longest diameter of the biopsied lesion with a measurement of 54.6 mm at baseline (**E**) and 34.2 mm after 3 months (**F**) of pembrolizumab and chemotherapy treatment

samples pose a risk of misinterpretation, potentially appearing as non-responders and introducing false negatives. Colorimetric assays to assess viability can be integrated into the platform to mitigate this, although they may negatively affect the tissue over time [28]. Adding a viability assay downstream of sequential treatment may be an approach to mitigate the negative effects of these assays; however the effects of treatment on this assay need to be elucidated. A better approach that is dye-free and non-invasive would be the use of dOCM, which detects intracellular movement to assess tissue viability. When integrated at the assay start, dOCM could enable the exclusion of necrotic samples from analysis. Second, the presence of tumor-free samples, another source of potential false-negatives, necessitates careful identification. While currently reliant on histological assessment, future advancements in imaging technologies may offer more efficient solutions for excluding samples lacking tumor content. Finally, collecting CNBs from a tumor may not always accurately reflect the potential for the patient's tumor to respond to ICI due to intratumor heterogeneity. In addition, CNBs are not always collected across multiple lesions. Previous studies have demonstrated differential ex vivo responses to ICI from within a tumor as well as across multiple lesions within a patient [16]. Ideally, the entire tumor would be assessed when possible, and it is critical to assess all available biopsy tissue to mitigate tumor heterogeneity. Additionally, a positive control for T-cell presence—such as αCD3/αCD28 stimulation following ICI treatment—could mitigate this risk to some extent, confirming the presence of functional T cells and a non-response to ex vivo ICI treatment.

Although histological biomarkers are routinely used in clinical practice, there are multiple reasons to suggest

that this platform may offer improved predictive accuracy for immunotherapy response compared with current biomarkers such as PD-L1. First, the use of a sequential treatment strategy enables assessment of ICI response across the entire CNB, in contrast to histological analysis, which typically evaluates only a fraction of the CNB tissue. Second, the distribution and expression level of PD-L1 vary across tumor types, creating challenges in establishing reliable thresholds for ICI treatment and contributing to variability in predictive value between cancers [37–39]. Data reported here, and in Voabil et al., support that the ex vivo assessment of cytokine response to immunotherapy is tumor agnostic, potentially broadening the clinical utility of the platform beyond that currently possible using PD-L1. Finally, the predictive accuracy of established biomarkers is limited by the lack of functional interaction of components within the native 3D TME in response to treatment—an advantage provided by this platform. Future studies comparing biomarker status to ex vivo LTF platform response will measure the potential for increased predictive accuracy of this platform compared to currently approved biomarkers.

Other ex vivo models for predicting ICI response preserve the native TME to varying degrees. Air-liquid interface organoids preserve the intratumoral T-cell repertoire and have been shown to upregulate IFNγ, granzyme B, and perforin following PD-1 blockade [40]. However, such organoid models often involve expansion of cells in culture, requiring additional time and limiting their clinical utility for guiding treatment decisions. Tumor fragment models derived from surgical resections also preserve the native TME and allow cytokine-based assessment of response [13, 16, 17]. These models rely on pooling large tissue amounts to mitigate heterogeneity and are not compatible with biopsies, thereby excluding patients with unresectable, advanced and metastatic disease—the population most likely to receive ICI therapy—from potential evaluation.

The sequential treatment strategy presented here enables detection of cytokine changes in response to ICI exposure in CNBs. Ongoing clinical studies are targeted to enroll over 600 patients and designed to evaluate the extent of correlation between ex vivo cytokine response on this platform and clinical outcomes, validating this approach as a predictive tool (ClinicalTrials.gov identifiers: NCT05478538, NCT05520099, NCT06349642). By leveraging CNBs and a sequential treatment design, the platform supports longitudinal profiling of tumor response and offers a practical method for guiding personalized ICI therapy. Importantly, this approach is not limited to ICI. The platform also has the potential to evaluate other immunotherapy modalities, including immune cell–based therapies and combination regimens, expanding the platform's clinical utility. Further studies are ongoing to explore these opportunities and validate use beyond ICI treatment.

Abbreviations

αPD-1	Anti-programmed cell death 1
αPD-L1	Anti-programmed cell death 1 ligand-1
CCK8	Cell counting kit 8
CDx	Companion diagnostic
CNB	Core needle biopsy
CTLA-4	Cytotoxic T-lymphocyte-associated protein 4
CV	Coefficient of variation
CXCL10	C-X-C motif chemokine ligand 10
dMMR	Mismatch repair deficiency
dOCM	Dynamic Optical Coherence Microscopy
FC	Fold change
FDA	Food and Drug Administration
H&E	Hematoxylin and eosin
ICI	Immune checkpoint inhibitor
IFNγ	Interferon gamma IgG
IgG	Immunoglobulin G
IHC	Immunohistochemistry
IL-1Ra	Interleukin-1 receptor agonist
LDH	Lactate dehydrogenase
LLOQ	Lower limit of quantitation
LTF	Live tumor fragment
MAD	Median absolute deviation
mIF	Multiplexed immunofluorescence
MMR	Mismatch repair
MSI	Microsatellite instability
NAD(P)H	Nicotinamide adenine dinucleotide phosphate
NSCLC	Non-small cell lung cancer
PDX	Patient-derived xenograft
pMMR	Mismatch repair proficiency
RECIST	Response Evaluation Criteria in Solid Tumors
TME	Tumor microenvironment

Supplementary Information

The online version contains supplementary material available at https://doi.org/10.1186/s12967-025-07378-2.

Supplementary Material 1

Supplementary Material 2

Acknowledgements

This paper is dedicated in the memory of Abhijeet Prasad, who made significant contributions to this work. We express our sincere gratitude to the patients, clinical staff, and researchers at participating clinical sites, including, Baylor Scott & White Health, CARTI Cancer Center, Mayo Clinic, Orlando Heath, The University of North Carolina, and The University of Wisconsin–Madison Department of Radiology, as well as to current and former Elephas employees and scientific collaborators, for their valuable contributions to this work. Some tissue samples were provided by the Cooperative Human Tissue Network which is funded by the National Cancer Institute. The authors thank the University of Wisconsin Carbone Cancer Center BioBank, supported by P30 CA014520, for use of its facilities and services, AARI & Biorepository and Specimen Resource Core, and Mercy Research located at Mercy Sindelar Cancer Center led by principal investigator Peter DiPasco, MD. The authors acknowledge the support of The University of Kansas Cancer Center's Biospecimen Repository Core Facility staff, funded in part by the National Cancer Institute Cancer Center Support Grant P30 CA168524; The University of Louisville, Division of Surgical Oncology Biobank; and The University of Tennessee Medical Center's Biobank for its service in providing biospecimens under the direction of Antje Bruckbauer, MD, PhD.

Author contributions

Conceptualization: TSR, SC, LCV, LCFH, MK, SJ, JO, HG. Methodology: TSR, PA, CMS, CJ, SC, CB, VB, EF, MK, AP. Formal analysis: TSR, PA, CMS, SC, LCV, ND, VB,

EF, MK, CS, EW, YL. Investigation: CMS, CJ, VB, YC, TD, EF, NK, AK, MK, NM, PM, AN, VP, AP, JR, SS, MMS, AS, EW, EEW, YL. Visualization: PA, CMS, CJ, SC, LCV, YL. Project administration: LCFH, CMS, SC, LCV. Supervision: TSR, LCFH, CMS, SC, NK, MK, CL, MMS, CS, SJ, JO, HG. Writing – original draft: TSR, PA, CMS, CJ, SC, LCV, ND, VB, EvE, MK, PM, HG. Writing – review & editing: TSR, PA, CMS, CJ, SC, LCFH, LCV, ND, CB, VB, YC, TD, EF, NK, AK, MK, CL, NM, PM, AN, VP, JR, SS, MMS, CS, AS, EvE, EEW, PA, BB, AB, AG, NK, YL RM, MR, GT, JR, AF, KE, MS, SJ, JO, JG, CC, DM, JT, DB, HG.

Funding
This work was fully funded by Elephas.

Data availability
The datasets used and/or analyzed during the current study are available from the corresponding author on reasonable request.

Declarations

Ethics approval and consent to participate
Experiments using murine models were performed in accordance with the Institutional Animal Care and Use Committee–approved protocol (23–003) in an Association for Assessment and Accreditation of Laboratory Animal Care International accredited laboratory. Protocols for the collection of human specimens were approved by an institutional review board by a waiver of consent or informed consent.

Consent for publication
Not applicable.

Competing interests
TSR, CMS, PA, CJ, SC, LCFH, LV, ND, CB, TB, YC, TD, EF, NK, AK, MK, CL, NM, PD, AN, VP, JR, SS, MMS, CS, AS, EvE, EW, EEW, JR, MS, SJ, JO, and HJG are employed by Elephas. TSR, CMS, PA, CJ, SC, LCFH, LV, ND, CB, TB, YC, TD, EF, NK, AK, MK, CL, NM, PD, AN, VP, JR., SS, MS, CS, AS, EW, EEW, JR, MS, SJ, JO, AF, KE, and HJG hold Elephas stock options. TSR, PA, SC, MK, and SJ, hold U.S. Patent App. No. 19/038,52. AF, KE, CC, JT, DB, and JG, receive consulting fees from Elephas. DM received travel funds from Elephas.

Author details
[1]Elephas Biosciences, 1 Erdman Place, Madison, WI 53717, USA
[2]Mayo Clinic, Jacksonville, FL, USA
[3]Orlando Health, Orlando, FL, USA
[4]The University of Tennessee Medical Center, Knoxville, TN, USA
[5]The University of Kansas Cancer Center, Kansas City, KS, USA
[6]University of North Carolina, Chapel Hill, NC, USA
[7]University of Louisville, Louisville, KY, USA
[8]Advocate Aurora Research Institute, Milwaukee, WI, USA
[9]University of Wisconsin, Madison, WI, USA
[10]Midwestern University, Glendale, AZ, USA
[11]Institute National de la Santé et de la Recherche Médicale, Paris, France
[12]John Hopkins University, Baltimore, MD, USA
[13]Yale School of Medicine, New Haven, CT, USA

Received: 22 August 2025 / Accepted: 23 October 2025
Published online: 03 January 2026

References

1. Sharma P, Goswami S, Raychaudhuri D, Siddiqui BA, Singh P, Nagarajan A, et al. Immune checkpoint therapy—current perspectives and future directions. Cell. 2023, Apr;186(8):1652–69.
2. Topalian SL, Hodi FS, Brahmer JR, Gettinger SN, Smith DC, McDermott DF, et al. Safety, activity, and immune correlates of anti–PD-1 antibody in cancer. N Engl J Med. 2012, Jun, 28;366(26):2443–54.
3. Taube JM, Klein A, Brahmer JR, Xu H, Pan X, Kim JH, et al. Association of PD-1, PD-1 ligands, and other features of the tumor immune microenvironment with response to anti–PD-1 therapy. Clin Cancer Res. 2014, Oct, 1;20(19):5064–74.
4. Garon EB, Rizvi NA, Hui R, Leighl N, Balmanoukian AS, Eder JP, et al. Pembrolizumab for the treatment of non–small-Cell lung cancer. N Engl J Med. 2015, May, 21;372(21):2018–28.
5. Le DT, Uram JN, Wang H, Bartlett BR, Kemberling H, Eyring AD, et al. PD-1 blockade in tumors with Mismatch-Repair Deficiency. N Engl J Med. 2015, Jun, 25;372(26):2509–20.
6. Patel SP, Kurzrock R. PD-L1 expression as a predictive biomarker in cancer immunotherapy. Mol Cancer Ther. 2015, Apr, 1;14(4):847–56.
7. Ratovomanana T, Nicolle R, Cohen R, Diehl A, Siret A, Letourneur Q, et al. Prediction of response to immune checkpoint blockade in patients with metastatic colorectal cancer with microsatellite instability. Ann Oncol. 2023, Aug;34(8):703–13.
8. Marabelle A, Fakih M, Lopez J, Shah M, Shapira-Frommer R, Nakagawa K, et al. Association of tumour mutational burden with outcomes in patients with advanced solid tumours treated with pembrolizumab: prospective biomarker analysis of the multicohort, open-label, phase 2 KEYNOTE-158 study. The Lancet Oncol. 2020, Oct;21(10):1353–65.
9. Haslam A, Olivier T, Prasad V. How many people in the us are eligible for and respond to checkpoint inhibitors: an empirical analysis. Int. J. Cancer. 2025, Jun, 15;156(12):2352–59.
10. Chen PL, Roh W, Reuben A, Cooper ZA, Spencer CN, Prieto PA, et al. Analysis of immune signatures in longitudinal tumor samples yields insight into biomarkers of response and mechanisms of resistance to immune checkpoint blockade. Cancer Discov. 2016, Aug, 1;6(8):827–37.
11. Ramos-Casals M, Brahmer JR, Callahan MK, Flores-Chávez A, Keegan N, Khamashta MA, et al. Immune-related adverse events of checkpoint inhibitors. Nat Rev Dis Primer. 2020, May, 7;6(1):38.
12. Yu X, Zhang X, Yao T, Zhang Y, Zhang Y. Fatal adverse events associated with immune checkpoint inhibitors in non–small cell lung cancer: a systematic review and meta-analysis. Front Med. 2021, Feb, 15;8:627089.
13. Jenkins RW, Aref AR, Lizotte PH, Ivanova E, Stinson S, Zhou CW, et al. Ex vivo profiling of PD-1 blockade using organotypic tumor spheroids. Cancer Discov. 2018, Feb, 1;8(2):196–215.
14. Sivakumar R, Chan M, Shin JS, Nishida-Aoki N, Kenerson HL, Elemento O, et al. Organotypic tumor slice cultures provide a versatile platform for immuno-oncology and drug discovery. OncoImmunology. 2019, Dec, 2;8(12):e1670019.
15. Roelants C, Pillet C, Franquet Q, Sarrazin C, Peilleron N, Giacosa S, et al. Ex-Vivo treatment of tumor tissue slices as a predictive preclinical method to evaluate targeted therapies for patients with renal carcinoma. Cancers. 2020, Jan, 17;12(1):232.
16. Voabil P, De Bruijn M, Roelofsen LM, Hendriks SH, Brokamp S, Van Den Braber M, et al. An ex vivo tumor fragment platform to dissect response to PD-1 blockade in cancer. Nat Med. 2021, Jul;27(7):1250–61.
17. Basak NP, Jaganathan K, Das B, Muthusamy O, R M, Malhotra R, et al. Tumor histoculture captures the dynamic interactions between tumor and immune components in response to anti-PD1 in head and neck cancer. Nat Commun [Internet]. 2024, Feb, 21;15(1). Available from: https://www.nature.com/articles/s41467-024-45723-z. cited 2025 May 23.
18. Majumder B, Baraneedharan U, Thiyagarajan S, Radhakrishnan P, Narasimhan H, Dhandapani M, et al. Predicting clinical response to anticancer drugs using an ex vivo platform that captures tumour heterogeneity. Nat Commun. 2015, Feb, 27;6(1):6169.
19. Fidler IJ, Hart IR. Biological diversity in metastatic neoplasms: origins and implications. Science. 1982, Sep, 10;217(4564):998–1003.
20. Marusyk A, Polyak K. Tumor heterogeneity: causes and consequences. Biochim Biophys Acta BBA - Rev Cancer. 2010, Jan;1805(1):105–17.
21. Vitale I, Shema E, Loi S, Galluzzi L. Intratumoral heterogeneity in cancer progression and response to immunotherapy. Nat Med. 2021, Feb;27(2):212–24.
22. Garber JC, Barbee RW, Bielitzki JT, Clayton LA, Donovan JC, Kohn DF, et al. Guide for the care and use of laboratory animals. 2011. http://www.nap.edu/catalog/12910. cited 2025 May 15]. Available from: Eighth Edition [Internet]. Washington, D.C.: National Academies Press.
23. Liu CJ, Smith JT, Wang Y, Ouellette JN, Rogers JD, Oliner JD, et al. Assessing cell viability with dynamic optical coherence microscopy. Biomed Opt Express. 2024, Mar, 1;15(3):1408.
24. Virtanen P, Gommers R, Oliphant TE, Haberland M, Reddy T, Cournapeau D, et al. SciPy 1.0: fundamental algorithms for scientific computing in Python. Nat Methods. 2020, Mar, 2;17(3):261–72.
25. Iglewicz B, Hoaglin DC. How to detect and handle outliers. Milwaukee, Wis: ASQC Quality Press; 1993. p. 87 p. (ASQC basic references in quality control.

26. Helmlinger G, Yuan F, Dellian M, Jain RK. Interstitial pH and pO2 gradients in solid tumors in vivo: high-resolution measurements reveal a lack of correlation. Nat Med. 1997, Feb;3:177–82.
27. Tominaga H, Ishiyama M, Ohseto F, Sasamoto K, Hamamoto T, Suzuki K, et al. A water-soluble tetrazolium salt useful for colorimetric cell viability assay. Anal Commun. 1999;36(2):47–50.
28. Fan J, Schiemer T, Vaska A, Jahed V, Klavins K. Cell via cell viability assay changes cellular metabolic characteristics by intervening with Glycolysis and pentose phosphate pathway. Chem Res Toxicol. 2024, Feb, 19;37(2):208–11.
29. Law AMK, Chen J, Colino-Sanguino Y, Fuente LRDL, Fang G, Grimes SM, et al. Alten: a High-Fidelity primary Tissue-Engineering platform to assess cellular responses ex vivo. Adv Sci [Internet]. 2022, Jul;9(21). Available from: https://onlinelibrary.wiley.com/doi/10.1002/advs.202103332. cited 2025 May 23.
30. Song J, Wei R, Liu C, Zhao Z, Liu X, Wang Y, et al. Antigen-presenting cancer associated fibroblasts enhance antitumor immunity and predict immunotherapy response. Nat Commun. 2025, Mar, 4;16(1):2175.
31. Arlauckas SP, Garris CS, Kohler RH, Kitaoka M, Cuccarese MF, Yang KS, et al. In vivo imaging reveals a tumor-associated macrophage–mediated resistance pathway in anti–PD-1 therapy. Sci Transl Med. 2017, May, 10;9(389):eaal3604.
32. Jiang P, Gu S, Pan D, Fu J, Sahu A, Hu X, et al. Signatures of T cell dysfunction and exclusion predict cancer immunotherapy response. Nat Med. 2018, Oct;24(10):1550–58.
33. Vinay DS, Ryan EP, Pawelec G, Talib WH, Stagg J, Elkord E, et al. Immune evasion in cancer: mechanistic basis and therapeutic strategies. Semin Cancer Biol. 2015, Dec;35:S185–98.
34. Wang X, Barrera C, Bera K, Viswanathan VS, Azarianpour-Esfahani S, Koyuncu C, et al. Spatial interplay patterns of cancer nuclei and tumor-infiltrating lymphocytes (TILs) predict clinical benefit for immune checkpoint inhibitors. Sci Adv. 2022, Jun, 3;8(22):eabn3966.
35. Gil-Jimenez A, Van Dijk N, Vos JL, Lubeck Y, Van Montfoort ML, Peters D, et al. Spatial relationships in the urothelial and head and neck tumor microenvironment predict response to combination immune checkpoint inhibitors. Nat Commun. 2024, Mar, 21;15(1):2538.
36. Moldoveanu D, Ramsay L, Lajoie M, Anderson-Trocme L, Lingrand M, Berry D, et al. Spatially mapping the immune landscape of melanoma using imaging mass cytometry. Sci Immunol [Internet]. 2022, Apr, 15;7(70). Available from: https://www.science.org/doi/10.1126/sciimmunol.abi5072. cited 2025 May 23.
37. Haragan A, Field JK, Davies MPA, Escriu C, Gruver A, Gosney JR. Heterogeneity of PD-L1 expression in non-small cell lung cancer: implications for specimen sampling in predicting treatment response. Lung Cancer. 2019, Aug;134:79–84.
38. Carbognin L, Pilotto S, Milella M, Vaccaro V, Brunelli M, Caliò A, et al. Differential activity of Nivolumab, Pembrolizumab and MPDL3280A according to the tumor expression of programmed death-ligand-1 (PD-L1): sensitivity analysis of trials in melanoma, lung and genitourinary cancers. PLoS One. 2015, Jun, 18;10(6):e0130142. Santini D, editor.
39. Kluger HM, Zito CR, Turcu G, Baine MK, Zhang H, Adeniran A, et al. PD-L1 studies across tumor types, its differential expression and predictive value in patients treated with immune checkpoint inhibitors. Clin Cancer Res. 2017, Aug, 1;23(15):4270–79.
40. Neal JT, Li X, Zhu J, Giangarra V, Grzeskowiak CL, Ju J, et al. Organoid modeling of the tumor immune microenvironment. Cell. 2018, Dec;175(7):1972–88.e16.

Publisher's Note